

# CO catalytic oxidation on Pt-doped single wall boron nitride nanotube: first-principles investigations



S. Abdel Aal \*

Department of Chemistry, Faculty of Science, Benha University, P.O. Box 13518, Benha, Egypt

Department of Chemistry, Faculty of Science and Arts, Qassim University, P.O. Box 6666, Qassim, Buraidah, Saudi Arabia

## ARTICLE INFO

### Article history:

Received 19 May 2015

Accepted 19 August 2015

Available online 29 August 2015

### Keywords:

DFT

Pt-doped BNNT

CO oxidation

Reaction mechanism

## ABSTRACT

The catalytic oxidation of CO at Pt-doped BNNT (5,5) has been investigated theoretically using density functional theory. The electronic structures and thermochemical properties of CO and O<sub>2</sub> that adsorbed on Pt embedded at the B- and N-vacancy sites of BNNTs are analyzed. It is demonstrated that the different BNNT substrates can modify the electronic structure of the Pt catalysts and cause different effects in the catalytic activities. With the N-vacancy (Pt<sub>(N)</sub>-BNNT), the Pt behaves as a Lewis acid for accepting an electron from the substrate, thus O<sub>2</sub> binds stronger than CO molecules, thus alleviating the CO poisoning of the platinum catalysts. Coadsorption of CO and O<sub>2</sub> on Pt<sub>(N)</sub>-BNNT results in additional charge transfer to O<sub>2</sub>. CO oxidation proceeds via the Eley–Rideal (ER) mechanism entails lower activation barrier and higher reaction rate than that of Langmuir–Hinshelwood (LH) mechanism suggesting the superiority of the ER mechanism for CO oxidation at Pt<sub>(N)</sub>-BNNT. Therefore, Pt<sub>(N)</sub>-BNNT might be a good candidate for low-cost, highly active, and stable catalysts for CO oxidation.

© 2015 Elsevier B.V. All rights reserved.

## 1. Introduction

The catalytic oxidation of carbon monoxide (CO) has attracted great interest not only for its important role in emission control of environmentally-harmful pollutants, but also for CO<sub>2</sub> lasers [1,2], removing CO from hydrogen gas fuel to avoid electrode poisoning in fuel cells [3], prototypical heterogeneous catalytic reaction in surface chemistry that plays an essential role in evaluating activity [4–6], selectivity and durability of a catalyst. Therefore, plentiful efforts have been devoted to design efficient catalyst for converting CO to eco-benign CO<sub>2</sub> molecule [7]. Deposited nanoparticles (NPs) of transition metals (TMs), such as Pt [8,9], Pd [10,11], Rh [6] and Au [12], can catalyze CO oxidation making them attractive candidates for next generation catalysts. Also Pt surfaces have been studied efficient for CO oxidation such as Pt/FeO<sub>x</sub> [13] and Pt/Al<sub>2</sub>O<sub>3</sub> [14]. Furthermore, Al, Fe, Cu and Pt atoms embedded graphene have also been predicted to be highly effective for CO catalytic oxidation [15–20,7]. Metal subnanoclusters supported on a graphene sheet have been found to exhibit high activity for oxidation reactions [21]. Moreover, Fe, Ru, Cu, Pt and Au atoms supported by hexagonal boron nitride nanosheet (h-BN) have been investigated theoretically as a single metal catalysis for CO oxidation [22–27]. Decomposition of nitrous oxide on Fe-doped boron nitride nanotubes (BNNTs) has been examined [28]. These studies suggest a possible new direction in designing future catalysts with high efficiency.

BNNTs, the structural analogues of carbon nanotubes (CNTs), have been the subject of extensive research in recent years. Unlike CNTs, BNNTs have a very large band gap (~5.5 eV) that is almost independent of the tube diameter, chirality, and number of walls. Moreover, BNNTs exhibit excellent mechanical properties, high thermal stability, high thermal conductivity, outstanding chemical stability and high oxidation resistivity [13,20,28–30]. However, the poor electrical conductivity and chemical inertness of pristine BNNTs might hinder their potential application in the development of gas sensors, catalysts and electronic devices [31–35]. Moreover, the ionic character of B–N bonds and possible vacancy defects benefit for BNNT as a support for heterogeneous catalysts. BN-nanotubes present a great opportunity to modify the catalytic activity of supported metal atom catalyst, even superior to CNT [24]. Some common defects at BNNT such as vacancies and Stone–Wales defects were experimentally identified [36,37]. H. Roohi et al. [38] found that the structural properties and formation energies of the single vacancies, divacancies, and Stone–Wales defects in BN nanotubes are dependent on the tube diameter as well as the length of the tube. Previous theoretical and experimental [39–42] studies indicate that the formation energy of a boron monovacancy is greater than that of a nitrogen monovacancy, thus the probability of nitrogen monovacancy is higher than the boron vacancy that is opposite to the results of Jin et al. [43]. Therefore, nitrogen vacancy (V<sub>N</sub>) is considered as one of the most interesting and intriguing type of point defects in BNNTs, because it may control electrical [44], magnetic [45], and optical [46] properties and can influence the hydrogen storage efficiency of BN nanotube [47]. The V<sub>N</sub> in BNNTs can be created by the low-energy ion bombardment, using argon and nitrogen ions [48]. In addition, the theoretical

\* Department of Chemistry, Faculty of Science, Benha University, P.O.Box 13518, Benha, Egypt. Tel.: +20 1002060932.

E-mail address: [safabdelaal11@yahoo.com](mailto:safabdelaal11@yahoo.com).

calculations demonstrated that BNNTs were changed from insulators to narrow band n- or p-type semiconductors through doping, [49–51] deformation, [52] and/or functionalization [53]. Meanwhile, the efficiency of gas adsorption on nanotubes can be enhanced by topological defects [54,55] or doping [56,57]. Strong binding energies between BNNTs and many TMs suggest BNNTs to be good candidates as the stationary phase in catalytic processes [58,59].

Very recently, theoretical results indicated that CO oxidation on Si–BNNT was very close with those on Si deposited h-BN, suggesting that these two Si-doped nanocomposites might exhibit similar catalytic activities [60]. On the other hand, Pt-stabilized by vacancy defects on h-BN demonstrated high catalytic activity for CO oxidation [18]. A. Zobelli et al. [37] reported that BNNTs were more susceptible to bear a monovacancy than h-BN. On the basis of the previous evidences, it is natural to expect that Pt embedded in defective BNNT can also exhibit a similar catalytic behavior. So that, in this work theoretical studies on the catalytic performance of Pt deposited at various defective BNNT in CO oxidation process will be examined using density functional theory (DFT).

## 2. Computational framework

First-principle calculations have been performed for CO oxidation on Pt-embedded boron nitride nanotube within the DFT method to shed light on the interaction mechanisms between the gas molecules and Pt-doped BNNT. The hybrid DFT with Becke's three parameter exchange functional [61] and the Lee–Yang–Parr correlation functional [62] have been used in the calculations. The pristine BNNT (5,5) and (7,7) with similar tube length 8 Å were constructed. The structure optimizations of the Pt-doped BNNT and their adsorption structures with CO and O<sub>2</sub> have been studied. In the case of (5,5) BNNT, 35 B and 35 N atoms with radius 3.54 Å and average bond length 1.47 Å was simulated. The chemical formula for Pt doping into the B and N single vacancies of (5,5) BNNTs were PtB<sub>34</sub>N<sub>35</sub> and PtB<sub>35</sub>N<sub>34</sub>, respectively. Also, the supercell with 98 boron–nitrogen atoms and radius 4.97 Å for the (7,7) BNNT was also simulated to study the effect of BNNT curvature (diameter) on the catalytic performance of Pt deposited at various sites of BNNT. The spin-unrestricted DFT calculations are performed which have been widely utilized for BNNT with functionalization of TMs.

All quantum chemical calculations based on the DFT/B3LYP method using the SDD basis set (Stuttgart/Dresden ECP plus DZ) were performed using GAUSSIAN 09 package [63]. The adsorption mechanisms are discussed in terms of the natural bond orbital (NBO) analysis and projected density of states (PDOSs) plots, which can provide a definitive description for charge redistribution. The PDOSs for the Pt-doped BNNT, their adsorptions structures with CO and O<sub>2</sub> and CO oxidation have been investigated. The PDOSs were plotted using the GaussSum 2.2.5 program [64] which is GUI utility tool to analyze the output from GAUSSIAN 09 calculations. The highest occupied molecular orbital (HOMO), the lowest unoccupied molecular orbital (LUMO) and the energy gaps referred to the energy difference between HOMO and LUMO orbitals ( $\Delta E_{\text{HOMO-LUMO}}$ ) were also investigated at the same level of theory. The molecular graphics of all related species were generated with the Gauss View 5.0 program.

## 3. Results and discussion

### 3.1. Adsorption of Pt on pristine and defective BNNTs

The reactivity of a single platinum atom on the surface of pristine, boron- and nitrogen-doped BNNTs (5,5) was investigated by calculating the binding energy of platinum atom on the various adsorption sites. The binding energy for the interaction Pt single atom on defective BNNT can be calculated as  $E_b(\text{Pt}) = [E(\text{Pt}/\text{BNNT\_site}) - E(\text{BNNT\_site}) - E(\text{Pt})]$ . In all cases, the negative values correspond to exothermic processes. The

binding of Pt atoms that is adsorbed on the B-vacancy ( $V_B$ ) and the N-vacancy ( $V_N$ ) sites of BNNT are  $-7.21$  and  $-6.76$  eV, respectively. The binding energies are strong enough to prohibit the diffusion and aggregation of the doped Pt atom. On the other hand, the interaction between a single Pt atom and the defect-free BNNT is investigated in this work with the adsorption energy of  $-1.34$  eV for Pt atom. Since the binding energy of Pt atom at defect free BNNT is significantly smaller than those at the defect sites, the defect sites are vital in producing stable Pt–BNNT. The calculated bond lengths are 1.94, 2.06, and 1.94 Å for the Pt–N bonds in the Pt– $V_B$  doped BNNT, and 2.00, 2.09 and 1.99 Å for the Pt–B bonds in the Pt– $V_N$  doped BNNT. The impurity Pt atom introduces the deformation of the six membered ring near the doping site to relieve stress resulting in the Pt protruding out of the tube wall due to the larger atomic radius of Pt than those of substituted B and N atoms, which is in agreement with the results regarding the substitution of metals onto the surface of boron nitride-based materials [65,66]. The vertical displacement of the Pt atom out of the BNNT is 1.201 and 1.247 Å for the Pt(<sub>B</sub>)–BNNT and Pt(<sub>N</sub>)–BNNT, respectively.

In contrast to the slightly negative partial charge accumulation on the platinum atom ( $q(\text{Pt}) = -0.19 e$ ) in the Pt N-doped BNNT, the Pt atom that substitutes a boron atom donates 0.89e toward its three bonding nitrogen atoms. The charge difference on the dopant Pt atom between the B-substitution and N-substitution doping cases can be explained by the electronegativity disparity between B and N atoms. The more electronegative N atom withdraws more electrons from the Pt atom at the B-substitution than the N-substitution doping.

It is observed that the replacement of Pt atom by either B atom ( $V_B$  site) or N atom ( $V_N$  site) leads to improve the conductivity of the BNNT. The pristine BNNTs, are essentially electrical insulation with the energy gap of 5.27 eV [28] can be tuned to a semiconducting character by doping Pt atom at the  $V_B$  site and  $V_N$  site with the band gap of 2.60 and 1.76 eV, respectively. Thus boron vacancy is more stable than nitrogen vacancy as shown by both experimental and theoretical [43,67]. Hence, the reactivity of the Pt adsorbed at the BNNT enhances due to the decreased band gap, and makes the system more conductive. Moreover, the Pt-functionalization of defective BNNT can induce attractive features, for example, rendering Pt as the active center in chemical reactions, and can react with approaching CO and O<sub>2</sub> molecules due to the higher chemical reactivity of embedded Pt atom.

The strong interaction between the embedded Pt atoms and defective BNNT can be further confirmed by PDOS (Figs. 1a and 2a). However, the contribution to the HOMO and LUMO in the Pt-embedded BNNT is mainly due to the Pt and its nearest neighboring atoms, the contributions from the other atoms are negligible. The PDOS of Pt-sp, Pt-d and N-sp states which localized on the Pt– $V_B$  are mainly contributed by the interaction between the in-plane components of Pt-d states (HOMO) and the N-sp states of N atoms that are surrounding the  $V_B$  site over a wide range of  $\sim -7.6$  eV. This suggests that Pt atom uses its valence states to interact with the defective states of the  $V_B$ . In the case of Pt(<sub>N</sub>)–BNNT (Fig. 2a), the LUMO that consists of Pt 6s and 6p orbitals is dominated by B-2p states of B atoms around the N-vacancy. Consequently, the overlap between the doped Pt atoms and the nearest B atoms at  $V_N$  is stronger than that of the nearest N atoms at  $V_B$  sites; which is consistent with [69].

Basically, like the CNTs, the electronic and mechanical properties for BNNTs with small size can be different from their large sized counterpart [68–71]. In order to explore the size-dependent features of defective BNNT that doping with Pt atoms, the calculations are extended to other considered (7,7) tubes with similar nanotube length. The results show that, the formation energy of B- and N-vacancy sites of BNNT with a smaller diameter (5,5) is lower than that with a larger diameter (7,7). This is in agreement with [29,68]. Instead, the bond lengths of both N–N and B–B bonds at the  $V_B$  and  $V_N$  defects in BNNT decrease very slightly as the diameter of the tube increases. As well as the ability of  $V_B$  and  $V_N$  defects in BN nanotubes to adsorb Pt decreases for nanotubes with larger diameters.

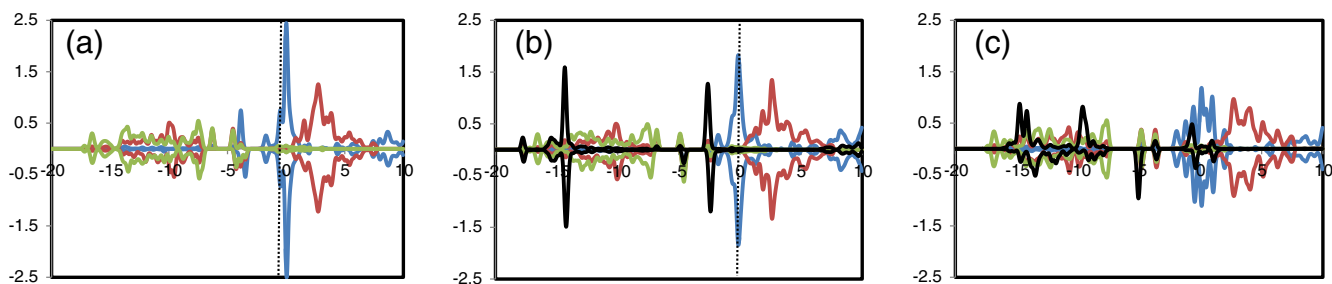


**Fig. 1.** The projected density of states (PDOS) of (a)  $\text{Pt}_{(\text{B})}$ -BNNT (b)  $\text{CO-Pt}_{(\text{B})}$ -BNNT (c)  $\text{O}_2\text{-Pt}_{(\text{B})}$ -BNNT. Pt-sp (blue) Pt-5d (red), N-2p (green), and CO or  $\text{O}_2$ -2p (black) orbitals in the Pt embedded BNNT with the B-vacancy. Spin-up ( $\uparrow$ ) and spin-down ( $\downarrow$ ) states are marked as positive and negative values, respectively. The Fermi level was set to zero.

On the other hand, to examine the influence of nanotube length on the formation energy of B- and N-vacancy sites and the Pt adsorption, a (5,5) BNNT with length (12 Å) was considered using a similar approach. It is demonstrated that as the tube length increases, the formation energy of  $V_{\text{B}}$  and  $V_{\text{N}}$  increases. The optimized geometric structure of the most stable long-tube (5,5) BNNT doped with Pt atom has been represented in Fig. 3. For comparison, the adsorption of Pt at shorter BNNT (8 Å) is greater than that of long-tube (5,5) BNNT (12 Å).

### 3.2. Adsorption of $\text{O}_2$ and CO on Pt-embedded BNNT

To investigate the oxidation of CO on Pt-doped BNNT, the adsorption of CO and  $\text{O}_2$  on Pt-doped BNNT was first examined. The optimized structures of CO and  $\text{O}_2$  complexes over  $\text{Pt}_{(\text{B})}$ -BNNT and  $\text{Pt}_{(\text{N})}$ -BNNT centers had been illustrated in Tables 1 and 2. The adsorption energies,  $E_{\text{b}}$ , for the different coverages of X (CO,  $\text{O}_2$ , O or  $\text{CO}_2$ ) are defined by the formula  $E_{\text{b}}(\text{X}) = [\text{E}(\text{X-Pt-BNNT\_site}) - \text{E}(\text{Pt-BNNT\_site}) - \text{E}(\text{X})]$ . Where  $\text{E}(\text{X-Pt-BNNT\_site})$  is the total energy of X (CO,  $\text{O}_2$ , O or  $\text{CO}_2$ ) that adsorbed at Pt-BNNT\_site system,  $\text{E}(\text{Pt-BNNT\_site})$  is the total energy of Pt atom trapped by the  $V_{\text{B}}$  or  $V_{\text{N}}$  at BNNT and  $\text{E}(\text{X})$  refers to total energy for isolated CO,  $\text{O}_2$ , O or  $\text{CO}_2$ . The geometrical parameters, binding energies and charge-transfer were represented in Tables 1 and 2. The results of these tables show that unlike the weak adsorption on pure-BNNT, CO molecule is chemisorbed on the Pt-doped BNNT forming the C–Pt bond that is tilted toward the nanotube surface. The arrangements of the adsorbed CO on Pt-embedded BNNT are consistent with that of on Pt-doped hexagonal boron nitride nanosheets [66] and the Pt on graphene [19]. It is observed that the interactions of CO molecules are stronger at the Pt that is deposited on the  $V_{\text{B}}$  site ( $E_{\text{b}} = -2.15$  eV) site than on the  $V_{\text{N}}$  site ( $E_{\text{b}} = -1.245$  eV), Tables 1 and 2. The distance between the CO and the Pt embedded at  $V_{\text{B}}$ -BNNT and  $V_{\text{N}}$ -BNNT was 1.94 and 2.03 Å, respectively suggesting the decrease in the interaction strength between the CO and the Pt-embedded at  $V_{\text{N}}$  itself. The lengths of the three Pt–N bonds in the optimized  $\text{OC-Pt}_{(\text{B})}$ -BNNT configuration are elongated to be 2.04, 1.94 and 2.04 Å and to be 2.03, 1.92 and 2.02 Å in the  $\text{OC-Pt}_{(\text{N})}$ -BNNT configuration indicating that the interaction of the Pt atom and the defective BNNT becomes relatively weak due to the chemical interaction between the CO molecule

and the Pt atom. The angle of Pt–C–O at  $V_{\text{B}}$  and  $V_{\text{N}}$  is  $176.6^\circ$  and  $174.0^\circ$  respectively. The C–O bond length (1.17 and 1.18 Å) is slightly longer than that of the isolated CO, indicating that adsorption process weakens the O–C bond of CO molecule [72].

NBO analyses demonstrate that maximum charge transferred from CO molecule to the Pt atom trapped by  $V_{\text{B}}$  and  $V_{\text{N}}$  are about 0.19 and 0.04 e, respectively. Therefore, the CO molecule acts as an electron donor and the embedded BNNT acts as an electron acceptor in the adsorption processes. The total charge transfer at B-vacancy is significantly larger than at N-vacancy, that may be result from the electron attracting ability of neighboring nitrogen atoms is stronger than that of boron atoms. Due to the adsorption of CO molecule, the band gap of the  $\text{OC-Pt}_{(\text{B})}$ -BNNT system increases to 1.91 eV however at  $\text{OC-Pt}_{(\text{N})}$ -BNNT system it reduced to 1.83 eV.

It is well-known that CO molecule is widely used as a probe molecule to explore the surface properties of catalysts and the interaction between adsorbates and catalysts because its vibration is sensitive to the nature of the adsorption sites. It has also been reported that the CO surface coverage and surface charge properties [73,74] can influence the CO frequencies. The calculated IR bands, Raman, force constants, dipole strengths, P- and U-depolarization spectra of CO complexes are collected in Table 3. The linear CO frequency which adsorbed at  $\text{Pt}_{(\text{B})}$ -BNNT is at  $2023.4 \text{ cm}^{-1}$ . However, the negative charge was assigned to Pt doped at  $V_{\text{N}}$ -BNNT gives rise to the CO frequency shifts to  $1921.0 \text{ cm}^{-1}$ , indicating that negative charge on Pt surface will lead to the red shift of CO frequency, P- and U-depolarization spectra. Meanwhile, the intensity of peak increased to some extent. Thus the nature and the location of the sites on which CO adsorb exhibits to various  $\nu$  (CO) bands.

Previous studies suggested that more than one molecule of CO should result in further stabilization as the coordination sites on the Pt center are becoming more saturated [75]. Geometry optimization has been carried out where two molecules of CO bonded to the Pt atom with the C-end orientation. It is demonstrated that two CO are adsorbed almost identically around the Pt atom that trapped by  $V_{\text{B}}$  or  $V_{\text{N}}$  as shown in Fig. 4, two CO molecules adsorbed in an almost symmetric fashion with average adsorption energies of  $-1.57$  and  $-1.00$  eV per CO molecule, forming a V-shape O–C–Pt–C–O structure at  $V_{\text{B}}$  and  $V_{\text{N}}$  sites respectively. The net energies released owing to the second adsorption

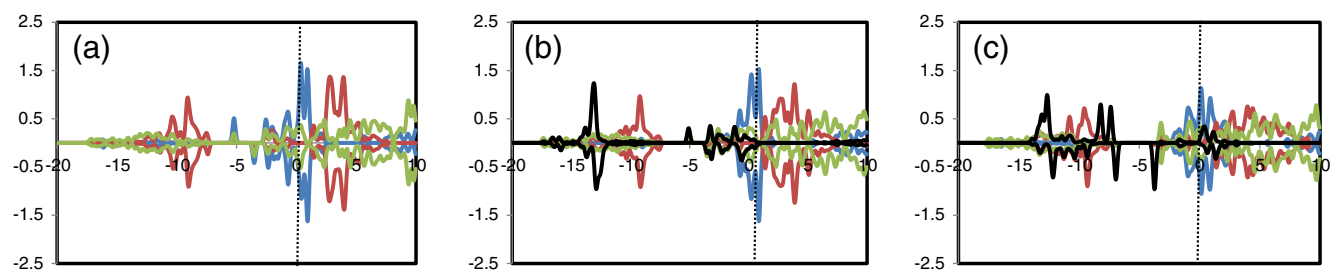


**Fig. 2.** The projected density of states (PDOS) of (a)  $\text{Pt}_{(\text{N})}$ -BNNT (b)  $\text{CO-Pt}_{(\text{N})}$ -BNNT (c)  $\text{O}_2\text{-Pt}_{(\text{N})}$ -BNNT. Pt-sp (blue) Pt-5d (red), B-2p (green), and CO or  $\text{O}_2$ -2p (black) orbitals in the Pt embedded BNNT with the N-vacancy. Spin-up ( $\uparrow$ ) and spin-down ( $\downarrow$ ) states are marked as positive and negative values, respectively. The Fermi level was set to zero.

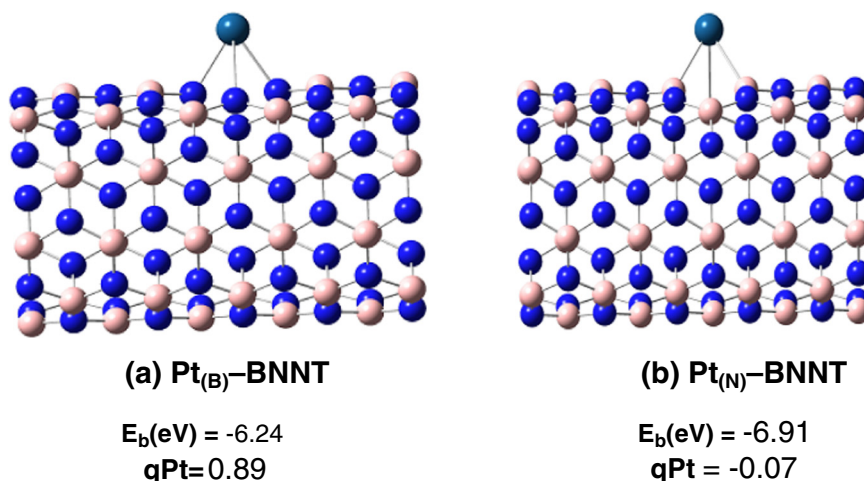


**Fig. 3.** Optimized structures, binding energy (eV) and charges (q) in a.u. for the Pt embedded in the defective BNNT (5,5) with tube length 12 Å.

were only  $-1.22$  and  $-0.88$  eV at Pt<sub>(B)</sub>-BNNT and Pt<sub>(N)</sub>-BNNT sites, respectively. These values are slightly below those for the adsorption of a single CO molecule due to the increased steric hindrance around the Pt center [75]. The energy gaps between the HOMO and LUMO have reverted to 2.56 and 2.29 eV for 2CO adsorbed at Pt<sub>(B)</sub>-BNNT and Pt<sub>(N)</sub>-BNNT, respectively. These band gaps are larger than those in the 1CO adsorbed at Pt-embedded BNNT, hence the conductivity and reactivity of the Pt-embedded BNNT decreases with one more CO adsorbed. The distance between the CO molecules and the Pt embedded at V<sub>B</sub>-BNNT and V<sub>N</sub>-BNNT has increased from 1.94 to 1.98 Å and from 2.05 to 2.06 Å, respectively indicating an overall decrease in the interaction

strength between the CO and the Pt-embedded BNNT. The back donation has also diminished to 0.19 at V<sub>B</sub> and 0.31 at V<sub>N</sub> for each CO. All attempts to coordinate three CO molecules to Pt-doped BNNT were unsuccessful, due to the increased steric bulk of the nanotube ligand; this is consistent with [75]. Consequently CO interaction can inhibit the gasification reaction due to the blockage of active sites.

Stationary points have been fully optimized and characterized by vibrational frequency calculations, which also provided zero point vibrational energies (ZPE), enthalpies (H) and Gibbs free energies (G). The vibrational frequency computations have been carried out at 298.15 K and standard pressure. Thermodynamic property changes ( $\Delta Z$ )

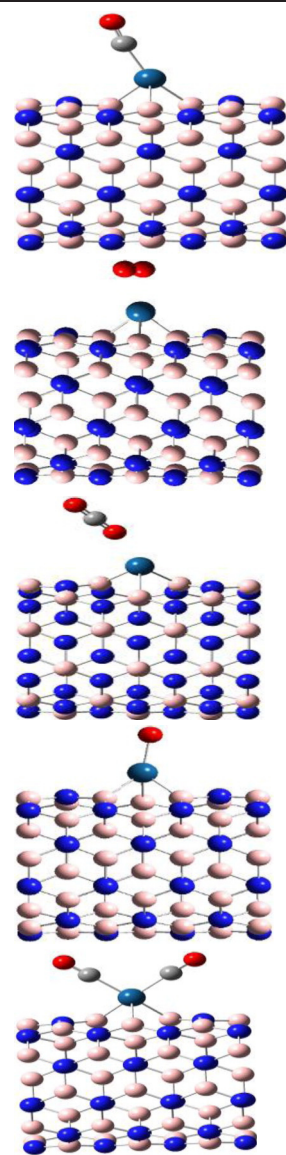
**Table 1**

Geometrical parameters (Å) binding energy (eV) and charges (q) in a.u. for Pt atom and X (CO, O<sub>2</sub>, 2CO) molecules at the Pt-embedded BNNT (5,5) with the B-vacancy.

Species	Bond details		$E_b(\text{eV})$	Charge details	
	Bond	Length (Å)		$q_{\text{Pt}}$	$q_{\text{X}}$
CO-Pt <sub>(B)</sub> -BNNT	C-O	1.17	-2.15	0.60	0.19
	Pt-C	1.94			
O <sub>2</sub> -Pt <sub>(B)</sub> -BNNT	O-O	1.35	-2.04	0.95	-0.31
	Pt-O	2.19			
	Pt-O	2.29			
2CO-Pt <sub>(B)</sub> -BNNT	Pt-C	1.98	-1.57	0.23	0.63
	Pt-C	1.98			
	C-O	1.17			
	C-O	1.17			

**Table 2**Geometrical parameters ( $\text{\AA}$ ) binding energy (eV) and charges (q) in a.u. for Pt atom and X (CO, 2CO, O<sub>2</sub>, O, CO<sub>2</sub>) molecules at the Pt-embedded in the BNNT (5,5) with the N-vacancy.

Species	Bond details		$E_b(\text{eV})$	Charge details	
	Bond	Length ( $\text{\AA}$ )		qPt	qX
CO-Pt <sub>(N)</sub> -BNNT	C–O	1.18	−1.25 (−1.25) <sup>c</sup>	−0.30	0.04
	Pt–C	2.03			
O <sub>2</sub> -Pt <sub>(N)</sub> -BNNT	O–O	1.41	−3.48 (−3.66) <sup>c</sup>	0.04	−0.48
	Pt–O	2.18			
	Pt–O	2.20			
CO <sub>2</sub> -Pt <sub>(N)</sub> -BNNT	Pt–O	2.48	−0.38	0.09	0.07
	C–O	1.20			
	C–O	1.18			
O-Pt <sub>(N)</sub> -BNNT	Pt–O	1.98	−5.37	0.01	−0.43
2CO-Pt <sub>(N)</sub> -BNNT	Pt–C	2.06	−1.00	−0.84	0.38 <sup>a</sup> 0.19 <sup>b</sup>
	Pt–C	2.06			
	C–O	1.16			
	C–O	1.16			

<sup>a</sup> Total charge transferred from 2CO molecules.<sup>b</sup> Total charge transferred from each CO molecule.<sup>c</sup> The end of BN nanotubes is saturated by hydrogen atoms.

i.e., Gibbs free energy ( $\Delta G^0$ ), enthalpy ( $\Delta H^0$ ) and zero point energy ( $\Delta E_{\text{ZPE}}$ ) changes of complexes can be calculated by equation  $\Delta Z = Z_p - Z_r$ , where  $Z_p$  are the thermodynamic properties of a products and  $Z_r$  are the thermodynamic properties of reactants. Therefore, to explore the effect of entropy and temperature on the adsorption processes,  $\Delta G^0$  were calculated at standard temperature and pressure

(STP, 1 atm. and 298 K), using B3LYP/SDD level which was used for optimizations. The results in Table 4 indicate that the adsorption process to form CO-Pt<sub>(B)</sub>-BNNT complex is an exothermic reaction ( $\Delta H^0 < 0$ ), with a negative  $\Delta G^0$  value of about  $-18.67$  for CO-Pt<sub>(B)</sub>-BNNT complex and  $0.46$  kcal/mol, respectively. In contrast the interaction of CO at Pt<sub>(N)</sub>-BNNT is less thermal stable at the same conditions.

**Table 3**

Infrared, Raman, force constant, infrared intensity, dipole strength, P- and U-depolarization spectra of CO at the Pt-embedded in the BNNT (5,5) with the B- and N-vacancy and two final steps of ER mechanism for CO-oxidation.

System	Infrared frequency ( $\text{cm}^{-1}$ )	Force constant (mDyne/ $\text{\AA}$ )	Infrared intensity	Dipole strength ( $10^{-40}$ esu <sup>2</sup> cm <sup>2</sup> )	Raman scattering activity (A <sub>2</sub> /AMU)	P-depol.	U-depol.
CO-Pt <sub>(N)</sub> -BNNT	1921.0	28.94	1503.4	3122.1	161.6	0.50	0.67
CO-Pt <sub>(B)</sub> -BNNT	2023.4	32.09	1063.2	2096.2	401.4	0.21	0.35
CO-O <sub>2</sub> -Pt <sub>(N)</sub> -BNNT (ER step 1)	2285.3	39.60	1093.7	1909.2	503.5	0.23	0.37
CO-O <sub>ads</sub> -Pt <sub>(N)</sub> -BNNT (ER step 2)	2313.2	40.59	1345.4	2320.3	1574.2	0.01	0.02

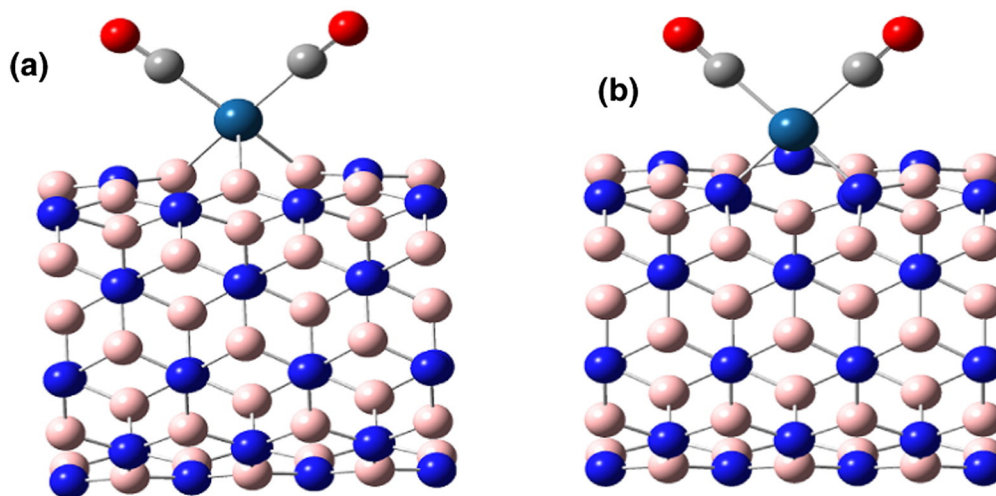


Fig. 4. Optimized structure of 2CO molecules adsorbed at (a)  $\text{Pt}_{(\text{N})}$ -BNNT and (b)  $\text{Pt}_{(\text{B})}$ -BNNT. Atoms are color labeled: B (pink), N (blue), Pt (cyan), O (red), and C (gray).

For the  $\text{O}_2$  molecule, another key reactant in CO oxidation, the preferred adsorption orientation is nearly parallel to the BNNT with two Pt–O bonds formed, rather different from CO. The results that presented in Tables 1 and 2 show that  $\text{O}_2$  adsorbs on  $\text{Pt}_{(\text{B})}$ -BNNT and  $\text{Pt}_{(\text{N})}$ -BNNT with the binding energies of  $-2.04$  and  $-3.48$  eV, respectively. The two Pt–O chemical bonds are formed with the bond distances of 2.20, 2.29 Å at  $V_{\text{B}}$ , slightly longer than that at  $V_{\text{N}}$  (2.18 and 2.20 Å). The O–O bond length in adsorbed  $\text{O}_2$  is enlarged similar to the superoxide state (the calculated O–O bond length in  $\text{O}^{-2}$  is 1.38 Å). NBO analysis reveals that 0.477 e and 0.31 e charge transfer from the  $\text{Pt}_{(\text{N})}$ -BNNT and  $\text{Pt}_{(\text{B})}$ -BNNT into the  $2\pi^*$  antibonding orbital of  $\text{O}_2$ , in agreement with the elongation of O–O bond length. The more pronounced charge transfer and the bond elongation of  $\text{O}_2$  on the  $\text{Pt}_{(\text{N})}$ -BNNT ( $-0.48$  e, 1.41 Å) than those on the  $\text{Pt}_{(\text{B})}$ -BNNT ( $-0.31$  e, 1.35 Å) suggest the stronger interaction of  $\text{O}_2$  on the  $\text{Pt}_{(\text{N})}$ -BNNT ( $E_{\text{b}} = -3.48$  eV) than that on the  $\text{Pt}_{(\text{B})}$ -BNNT ( $E_{\text{b}} = -2.04$  eV). Hence, the elongated O–O bond is correlated with transferring of electrons to  $\text{O}_2$ , i.e., the more charge transferred to  $\text{O}_2$  from the Pt doped BNNT systems; the more elongated the O–O bond lengths. This effect is essentially strong for the  $V_{\text{N}}$  defect that can act as an electron donor for the doped Pt atom. Obviously, these results give rise to speculate that the  $\text{O}_2$  molecule could be dissociated on the surface of Pt doped BNNT.

Table 4 shows the corresponding enthalpies and Gibbs free energies of  $\text{O}_2$  molecule at  $\text{Pt}_{(\text{B})}$ -BNNT and  $\text{Pt}_{(\text{N})}$ -BNNT complexes. It is observed that the high negative values of the thermodynamic parameters shown in Table 4 confirm the well-known fact that  $\text{O}_2$  chemisorption occurs readily on both  $\text{Pt}_{(\text{N})}$ -BNNT and  $\text{Pt}_{(\text{B})}$ -BNNT sites even at room temperature. This process, and especially its  $\text{O}_2$  dissociation step, is predicted to be more exothermic and more spontaneous on the  $\text{Pt}_{(\text{N})}$ -BNNT than on  $\text{Pt}_{(\text{B})}$ -BNNT counterpart.

To gain a deeper understanding of the interaction between the doped Pt atoms and adsorbate (CO or  $\text{O}_2$ ) the PDOSs are computed. As

evidenced by the PDOS (Figs. 1 and 2b,c), the hybridization between Pt-5d and CO-2p orbitals is weak near the Fermi level ( $E_{\text{F}}$ ). In contrast with the  $\text{Pt}_{(\text{N})}$ -BNNT, the Pt 5d peaks are slightly increased in the CO adsorbed at  $\text{Pt}_{(\text{B})}$ -BNNT due to the electronic charge transferred from the occupied CO 5 $\sigma$  states to Pt. Also, in comparison with the CO adsorption, a stronger overlap between the metal 5d orbitals and  $\text{O}_2$ -2p orbitals near  $E_{\text{F}}$  can be observed that is almost certainly responsible for the strong adsorption of  $\text{O}_2$  at the  $\text{Pt}_{(\text{N})}$ -BNNT and significant weakening of the O–O bond. Accordingly,  $\text{O}_2$  species can be efficiently activated by the  $\text{Pt}_{(\text{N})}$ -BNNT surface and the incoming CO molecule might readily react with the adsorbed  $\text{O}_2$  to produce  $\text{CO}_2$ , consequently enhancing the performance of the CO oxidation.

However, owing to the adsorption energy discrepancy, the Pt atom adsorbed at the nitrogen vacancy sites possesses a charge of  $-0.19$  e; but in the case of Pt adsorption on a  $V_{\text{B}}$ -BNNT center the charge localized on Pt is  $+0.89$  e. Thereby,  $V_{\text{N}}$  donates electrons to the adsorbed Pt, while  $V_{\text{B}}$  acts as an electron acceptor. The charge excess on the supported Pt atom results in a stronger binding of  $\text{O}_2$  to the Pt; while charge deficiency on Pt results in stronger binding of CO. Since the charge state of the supported Pt strongly influences the adsorption of  $\text{O}_2$  and CO, the defected BNNT supports dramatically affect  $\text{O}_2$  and CO adsorption to the supported Pt atoms. The calculated binding energies indicate that there might be a competition between the CO and  $\text{O}_2$  adsorption at the metal site. At the  $\text{Pt}_{(\text{N})}$ -BNNT, the  $\text{O}_2$  binds stronger than CO, the metal center will be overpopulated with the  $\text{O}_2$  species. Whereas at the  $\text{Pt}_{(\text{B})}$ -BNNT the metal site will be covered by CO which binds stronger than  $\text{O}_2$ , hence might poison the catalyst. Based on the present calculations,  $\text{O}_2$  is expected to preferentially occupy the Pt–N substitution allowing reaction with the incoming CO species via an Eley–Rideal (ER) type mechanism [67].

As shown in Table 2, the atomic O strongly interacts with the Pt- $V_{\text{N}}$ -BNNT yielding adsorption energy of  $-5.37$  eV and the distance between

Table 4  
Thermodynamic parameters of CO and  $\text{O}_2$  adsorption on Pt embedded-BNNT (5,5) and different pathways of oxidation of CO on the  $\text{Pt}_{(\text{N})}$ -BNNT surface.

Reaction	$\Delta G^0$	$\Delta H^0$	$\Delta S^0$	$\Delta E_{\text{ZPE}}^0$	$E_{\text{t}}$	$C_{\text{v}}$
$\text{CO} + \text{Pt}_{(\text{N})}$ -BNNT = CO- $\text{Pt}_{(\text{N})}$ -BNNT	0.46	-10.17	-34.49	-27.61	262.54	187.86
$\text{CO} + \text{Pt}_{(\text{B})}$ -BNNT = CO- $\text{Pt}_{(\text{B})}$ -BNNT	-18.67	-28.95	-35.66	-46.75	263.97	188.48
$\text{O}_2 + \text{Pt}_{(\text{N})}$ -BNNT = $\text{O}_2$ - $\text{Pt}_{(\text{N})}$ -BNNT	-70.62	-79.02	-47.02	-78.77	262.56	189.31
$\text{O}_2 + \text{Pt}_{(\text{B})}$ -BNNT = $\text{O}_2$ - $\text{Pt}_{(\text{B})}$ -BNNT	-61.72	-76.24	-37.58	-74.56	247.67	187.18
$\text{CO} + \text{O}_2$ - $\text{Pt}_{(\text{N})}$ -BNNT = $\text{CO}_2 + \text{O}_{\text{ads}}$ - $\text{Pt}_{(\text{N})}$ -BNNT	-33.67	-40.61	-23.29	-59.02	248.31	188.93
$\text{CO} + \text{O}_{\text{ads}}$ - $\text{Pt}_{(\text{N})}$ -BNNT = $\text{Pt}_{(\text{N})}$ -BNNT + $\text{CO}_2$	-21.52	-25.93	-14.80	-44.59	255.49	196.92

$\Delta G^0$  (kcal/mol), is the Gibbs free energy change of the process.  $\Delta H^0$  (kcal/mol), is the enthalpy change of the process.  $\Delta S^0$  (cal/mol K) is the entropy change of the process  $\Delta S^0 = (\Delta H^0 - \Delta G^0) / T$ .  $\Delta E_{\text{ZPE}}^0$  (kcal/mol), is the zero point vibrational energy change of the process. Thermal energy  $E_{\text{t}}$  (kcal/mol), and heat capacity at constant volume  $C_{\text{v}}$  (cal/mol K).

**Table 5**

Structural parameters and calculated activation energies for co-adsorption of CO and O<sub>2</sub> for the IS, TS and FS through the LH-mechanism of the CO oxidation on the Pt<sub>(N)</sub>-BNNT (5,5) along two reaction pathways (a) CO + O<sub>2</sub> → OOCO → CO<sub>2</sub> + O<sub>ads</sub> on Pt<sub>(N)</sub>-BNNT (b) CO + O<sub>ads</sub> → OCO → CO<sub>2</sub>, as displayed in Fig. 6.

	d(C–O)	d(O1–Pt)	d(O2–Pt)	d(C–Pt)	d(C–O2)	d(O1–O2)	∠O1–C–O	qPt	qO <sub>2</sub> /O	qCO	E <sub>b</sub>	E <sub>coads</sub> <sup>CO</sup>	ΔE	E <sub>bar</sub>
<i>(a)</i>														
LH-IS1	1.18	2.17	2.20	2.01	1.88	1.41	109.8	−0.11	−0.63	0.20	−4.87	−2.44	−3.12	1.04
LH-TS1	1.19	2.01	2.41	2.11	1.26	1.56	131.2	−0.12	−0.61	0.20				
LH-FS1	1.18	2.00	2.84	2.42	1.20	2.23	176.3	−0.11	−0.65	0.27				
<i>(b)</i>														
LH-IS2	1.18	2.10	–	1.98	3.00	–	119.5	−0.16	−0.67	0.08	−5.56	−2.13	−1.85	0.51
LH-TS2	1.20	2.11	–	2.24	1.87	–	123.1	−0.15	−0.39	−0.16				
LH-FS2	1.18	2.44	–	2.94	1.21	–	177.7	−0.12	−0.39	−0.06				

The activation energy barrier E<sub>bar</sub> is calculated with E<sub>bar</sub> = E<sub>TS</sub> − E<sub>IS</sub> and the reaction energy ΔE is calculated by ΔE = E<sub>FS</sub> − E<sub>IS</sub>, where IS, TS and FS are the initial, transition and final states, respectively. The reaction energy with positive and negative value represents endothermic and exothermic reactions, respectively.

O atom and doped-Pt is calculated to be 1.98 Å. In stark contrast to CO, O<sub>2</sub> and O, CO<sub>2</sub> is observed to physically adsorb above the Pt<sub>(N)</sub>-BNNT with an adsorption energy (−0.38 eV). Hence, as a final product, CO<sub>2</sub> can readily desorb from the Pt<sub>(N)</sub>-BNNT catalyst at the room temperature. In addition, the binding of CO<sub>2</sub> on the Pt<sub>(N)</sub>-BNNT (−0.38 eV) is smaller than that on the Pt on pristine BNNT (−0.87 eV), indicating that a CO<sub>2</sub> molecule is more facily desorbed from the Pt<sub>(N)</sub>-BNNT. Consequently, the Pt<sub>(N)</sub>-BNNT can strongly bind the reactants (O<sub>2</sub>, CO, and O atom), and release the CO<sub>2</sub> molecule easily, which may facilitate the CO oxidation.

The coadsorption energy of CO adsorbed on the Pt<sub>(N)</sub>-BNNT surface with pre-adsorbed O<sub>2</sub> molecule is calculating using the following expressions:

$$E_{\text{coads}}^{\text{CO}} = E(\text{CO} + \text{O}_2)/\text{Pt}_{(N)}\text{-BNNT} - E(\text{O}_2/\text{Pt}_{(N)}\text{-BNNT}) - \text{ECO}$$

$$E_{\text{coads}}^{\text{CO}} = E(\text{CO} + \text{O})/\text{Pt}_{(N)}\text{-BNNT} - E(\text{O}/\text{Pt}_{(N)}\text{-BNNT}) - \text{ECO}$$

where E(CO + O<sub>2</sub>) / Pt<sub>(N)</sub>-BNNT is the total energy of Pt<sub>(N)</sub>-BNNT − (CO + O<sub>2</sub>) system. E(O<sub>2</sub> / Pt<sub>(N)</sub>-BNNT) is the total energy of O<sub>2</sub> / Pt<sub>(N)</sub>-BNNT and ECO is the total energy for isolated CO molecule.

In addition, the binding E<sub>b</sub> of the coadsorbed species is calculated using the relation [76]:

$$E_b = E(\text{CO} + \text{O}_2)/\text{Pt}_{(N)}\text{-BNNT} - E(\text{Pt}_{(N)}\text{-BNNT}) - \text{ECO} - \text{EO}_2.$$

The binding energies of coadsorbed CO and O<sub>2</sub> at the Pt atom trapped by the V<sub>N</sub> defect (−5.30 eV) are more stable than the individual adsorption CO and O<sub>2</sub> on embedded Pt. This fact demonstrates the appearance of a cooperative effect in coadsorption of O<sub>2</sub> and CO, similar to those discussed in Refs [77–80] and references therein. Also, the coadsorption energy of CO at O<sub>2</sub>-Pt<sub>(N)</sub>-BNNT reaction site is found to be −2.67 eV, suggesting that it is energetically stable.

Tables 5 and 6 present the calculated charge localized on O<sub>2</sub> and CO molecules of the most stable configurations when CO and O<sub>2</sub> are coadsorbed on Pt<sub>(N)</sub>-BNNT center. The charge localized on O<sub>2</sub> is larger

than for the corresponding configurations without CO. It is interesting that in the case of O<sub>2</sub> and CO coadsorption on Pt trapped by a V<sub>N</sub> defect the extra charge on O<sub>2</sub> originates from the CO molecule itself, i.e., the CO molecule plays the role of an electron donor. The results reveal that pushing the system to the transition state makes the CO and O bands overlap and the product state PDOS has a clear molecular-like electronic structure of CO<sub>2</sub> with a double peak at −15 to −17 eV below Fermi level, Fig. 5. This is confirmed by the infrared results that are presented in Table 3 where the IR spectrum of carbon dioxide has a strong absorption band that caused by asymmetrical C=O stretching at about 2285.3 and 2313.2 cm<sup>−1</sup>. This result is consistent with [81]. Although, a continuous up shift of the IR bands, Raman scattering activity, force constants and dipole strength, a parallel down shift of infrared intensity, P- and U-depolarization spectra are observed under the effect of different BNNT sites.

To evaluate the effect of BNNT curvature (diameter) on CO and O<sub>2</sub> adsorption, a similar calculation procedures were investigated for a single Pt atom attached to the pristine, V<sub>B</sub> and V<sub>N</sub> defects on the BNNT (7,7). Table 7 shows the optimized geometric structure of the most configurations. The corresponding binding energies and depicted geometry structure data are listed in Table 7. Upon comparing the results obtained for the (5,5) and (7,7) BNNTs, it is demonstrated that the binding energies for the adsorption of CO and O<sub>2</sub> molecules at Pt doped to the various active sites of the BN-nanotube decrease with increasing BNNT diameter.

### 3.3. Reaction mechanisms for the CO oxidation

As a heterogeneous reaction, CO oxidation can be proceeding through two mechanisms: Langmuir–Hinshelwood (LH) mechanism and the Eley–Rideal (ER) mechanism, depending on the chemical nature of the catalysts [15–19,82,83]. The LH mechanism involves the coadsorption of O<sub>2</sub> and CO molecules before reaction. In the ER mechanism, the preadsorbed O<sub>2</sub> reacts directly with physisorbed CO molecule followed by the formation of an intermediate state and desorption of

**Table 6**

Structural parameters and calculated activation energies for co-adsorption of CO and O<sub>2</sub> for the IS, TS and FS through the ER-mechanism of the CO oxidation on the Pt<sub>(N)</sub>-BNNT along two reaction pathways (a) CO + O<sub>2</sub> → OOCO → CO<sub>2</sub> + O<sub>ads</sub> on Pt<sub>(N)</sub>-BNNT (5,5) (b) CO + O<sub>ads</sub> → OCO → CO<sub>2</sub>, as displayed in Figs. 5 and 7.

	d(C–O)	d(O1–Pt)	d(O2–Pt)	d(C–Pt)	d(C–O2)	d(O1–O2)	∠O1–C–O	qPt	qO <sub>2</sub> /O	qCO	E <sub>b</sub>	E <sub>coads</sub> <sup>CO</sup>	ΔE	E <sub>bar</sub>
<i>(a)</i>														
ER-IS1	1.15	2.18	2.20	4.65	2.80	1.41	119.2°	−0.01	(−0.47)	(0.01)	−5.30	−2.67	−3.63	0.37
ER-TS1	1.16	2.13	2.81	3.96	2.20	1.97	135.4°	0.00	(−0.55)	(0.06)				
ER-FS1	1.18	1.98	2.97	3.74	1.19	2.89	178.6°	0.01	(−0.99)	(0.57)				
<i>(b)</i>														
ER-IS2	1.16	1.98	–	4.37	3.07	–	122.0°	0.02	−0.44	(0.01)	−7.25	−1.88	−1.80	0.24
ER-TS2	1.18	2.06	–	3.22	1.79	–	135.6°	0.09	−0.72	(0.21)				
ER-FS2	1.18	3.31	–	3.84	1.19	–	179.6°	0.14	−0.58	(0.66)				

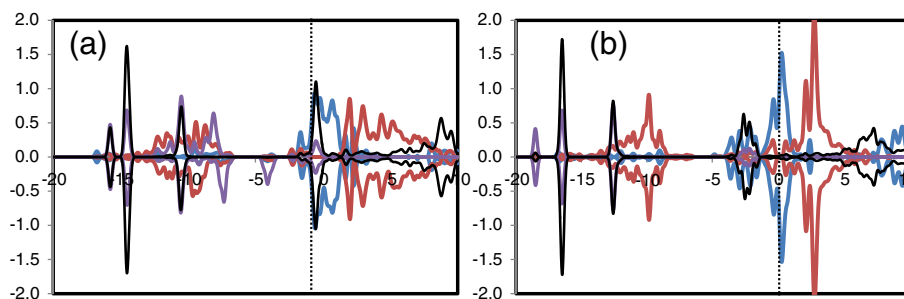


**Fig. 5.** The projected density of states (PDOS) of reaction (a)  $\text{CO} + \text{O}_2 \rightarrow \text{OOCO} \rightarrow \text{CO}_2 + \text{O}(\text{ads})$  on  $\text{Pt}_{(N)}\text{-BNNT}$  and reaction (b)  $\text{CO} + \text{O}(\text{ads}) \rightarrow \text{OCO} \rightarrow \text{CO}_2$ . Pt-sp (blue) Pt-3d (red), B-2p (green), and CO-2p (black) or  $\text{O}_2$ -2p (purple) orbitals in the Pt embedded BNNT with the N-vacancy. Spin-up ( $\uparrow$ ) and spin-down ( $\downarrow$ ) states are marked as positive and negative values, respectively. The Fermi level was set to zero.

$\text{CO}_2$  molecule. The larger adsorption energy of  $\text{O}_2$  ( $-3.48$  eV) compared with the CO ( $-1.25$  eV), and the elongated  $\text{O}_2$  bond on the  $\text{Pt}_{(N)}\text{-BNNT}$  ( $1.41$  Å) suggest the possible reaction process of CO oxidation by the ER mechanism. Although the difference in adsorption energy between CO and  $\text{O}_2$  is relatively large, the coadsorption energy of CO and  $\text{O}_2$  molecules ( $-2.67$  eV) indicates that there is a certain probability of having

$\text{O}_2$  and CO coadsorbed on  $\text{Pt}_{(N)}\text{-BNNT}$  as reported in literatures [16,18, 19]. Therefore, to clarify the preferred mechanism for CO oxidation on the  $\text{Pt}_{(N)}\text{-BNNT}$  substrate both mechanisms were investigated.

According to the LH mechanism, The configuration of coadsorbed CO and  $\text{O}_2$  on the  $\text{Pt}_{(N)}\text{-BNNT}$  is considered as the initial state (LH-IS1) in Fig. 6 where CO and  $\text{O}_2$  molecules are tilted and parallel to the  $\text{Pt}_{(N)}\text{-}$

**Table 7**

Geometrical parameters (Å) binding energy (eV) and charges (q) in a.u. for Pt atom and X (CO,  $\text{O}_2$ ) molecules at the Pt-embedded in the BNNT (7,7) with the B- and N-vacancy.

Species	Bond details		$E_b$ (eV)	Charge details	
	Bond	Length (Å)		qPt	qX
CO- $\text{Pt}_{(B)}$ -BNNT	C-O	1.16	-2.12	0.58	0.18
	Pt-C	1.97			
$\text{O}_2$ - $\text{Pt}_{(B)}$ -BNNT	O-O	1.30	-1.98	0.87	-0.27
	Pt-O	2.21			
	Pt-O	2.31			
CO- $\text{Pt}_{(N)}$ -BNNT	C-O	1.17	-1.11	-0.25	0.01
	Pt-C	2.05			
$\text{O}_2$ - $\text{Pt}_{(B)}$ -BNNT	O-O	1.36	-3.35	0.03	-0.39
	Pt-O	2.23			
	Pt-O	2.24			

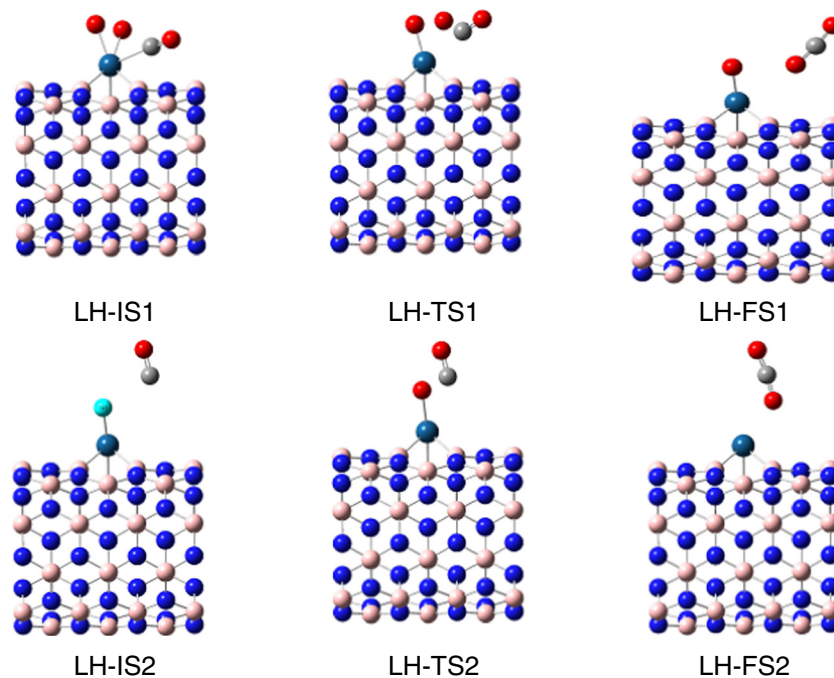


**Fig. 6.** Geometries of the initial state (IS), transition state (TS) and final state (FS) for two steps in LH-mechanism for the CO oxidation on the BNNT with Pt embedded in the N-vacancy.

BNNT surface, respectively. During this endothermic process, the O–O distance in  $O_2$  is elongated from 1.41 Å in LH-IS1 to 1.56 Å in LH-TS1 and one Pt–O bond is elongated from 2.20 to 2.41 Å to approach the carbon atom of CO and reach the transition state (LH-TS1). Hence a new C–O2 distance is shortened from 1.88 Å to 1.26 Å, implying the strengthening of the C–O2 interaction and the weakening of the O1–O2 and Pt–C interaction. After overcoming an energy barrier of 1.04 eV, a physisorbed  $CO_2$  and an O atom adsorbed on  $Pt_{(N)}$ -BNNT (LH-FS1) are produced. The subsequent reaction takes place between another gaseous CO molecule and the adsorbed atomic O1 adsorbed at  $Pt_{(N)}$ -BNNT (LH-IS2) to form a second physisorbed  $CO_2$  (LH-FS2) for the regeneration of Pt atom as available reaction center, see Fig. 6 and Table 5. Within LH-TS2, the Pt–CO distance is increased from 1.98 Å in LH-IS2 to 2.24 Å and the C–O1 distance is decreased from 3.00 to

1.87 Å due to the formation of an interaction between CO and preadsorbed O atom. As expected from the high reactivity of the adsorbed O atom (O1) and the strong exothermic formation of  $CO_2$ , the formation of LH-FS2 is exothermic by 1.85 eV with respect to LH-IS2. The corresponding energy barrier along the reaction pathway is estimated to be 0.51 eV.

Moreover, the ER mechanism is considered for CO oxidation as a probe of the catalytic activity of Pt-BNNT. The ER reaction proceeds as follows:  $Pt_{(N)}$ -BNNT +  $O_2$ (gas) + CO(gas)  $\rightarrow$   $Pt_{(N)}$ -BNNT- $O_2$ (ads) + CO(gas)  $\rightarrow$   $Pt_{(N)}$ -BNNT-O(ads) +  $CO_2$ (ads)  $\rightarrow$   $Pt_{(N)}$ -BNNT +  $CO_2$ (gas). The configurations for the initial state (IS), transition state (TS), and final state (FS) are displayed in Fig. 7. The corresponding binding energies and depicted geometry structure data of the three configurations are listed in Table 6 and Fig. 7. At ER-IS1 the adsorption energy and

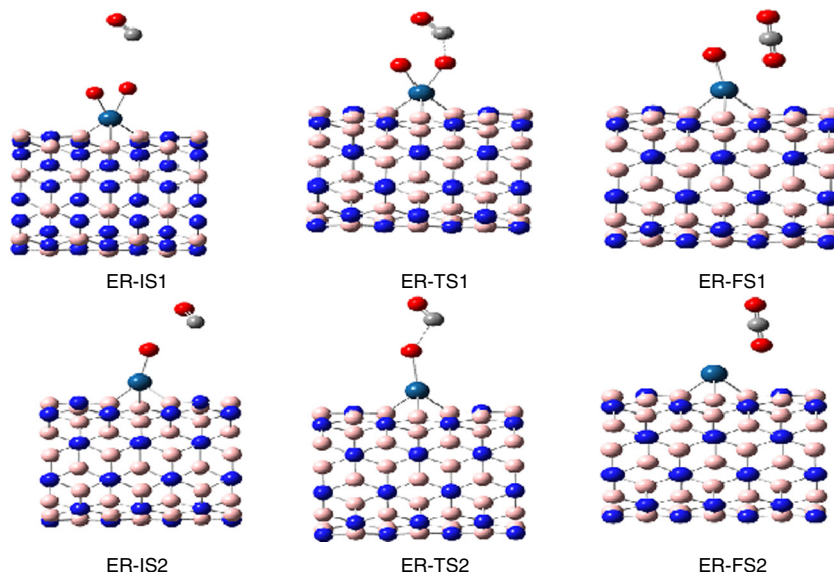


**Fig. 7.** Geometries of the initial state (IS), transition state (TS) and final state (FS) for two steps in ER-mechanism for the CO oxidation on the BNNT with Pt embedded in the N-vacancy.

**Table 8**  
Geometrical parameters (Å) binding energy (eV) and charges transfer of Pt<sub>2</sub> and Pt<sub>3</sub> Clusters at the B- and N-vacancy BNNT (5,5).

	E <sub>b</sub> (eV)	d <sub>Pt-B</sub>	d <sub>Pt-N</sub>	d <sub>Pt-Pt</sub>	Q <sub>Pt<sub>n</sub></sub>	
Pt <sub>2</sub> Defect free	-1.15	2.27	2.19	2.43	0.13	
V <sub>B</sub>	-7.264		1.96 2.08 1.99	2.49	0.64	
V <sub>N</sub>	-7.662	2.04 2.11 2.01		2.56	-0.36	
Pt <sub>3</sub> Defect free	-1.07	2.29	2.26	2.54 2.54 2.48	0.21	
V <sub>B</sub>	-6.718		1.99 2.10 2.02	2.63 2.62 2.46	0.73	
V <sub>N</sub>	-6.863	2.05 2.14 2.03		2.69 2.69 2.46	-0.37	

structure data, there is no interaction between CO and O<sub>2</sub>-Pt-V<sub>N</sub> system. At ER-TS1, the O1-O2 bond length was about 1.97 Å, and the distance of C-O2 decrease from 2.8 to 2.2 Å. At ER-FS1, the CO<sub>2</sub> molecule was formed with one oxygen atom (O1) adsorbed at Pt<sub>(N)</sub>-BNNT. The results are listed in Table 6 that reveal this exothermic reaction ( $\Delta E = -3.63$  eV) has an activation energy barrier of 0.37 eV. Furthermore, a second ER step has been investigated, in which CO is oxidized by the atomic oxygen atom O1, which is still existing after the generation of the first CO<sub>2</sub> product. In Fig. 7, a parallel orientation of the CO

more than 3.07 Å away from the preadsorbed O1 atom on Pt is chosen as the initial state (ER-IS2). At ER-TS2, CO molecule with the C-end orientation attacks the O1 atom with the C-O1 distance of 1.79 Å. At ER-FS2, a CO<sub>2</sub> molecule is formed above the reaction site where the distance of Pt-O1 enhanced to be 3.31 Å. The activation energy for this step is calculated to be 0.24 eV, which is slightly smaller than the generation of the first CO<sub>2</sub> and the exothermicity is -1.80 eV. Therefore, after CO<sub>2</sub> desorption, the Pt<sub>(N)</sub>-BNNT catalyst is recovered for a new cycle of CO oxidation.

The kinetic parameters are summarized in Table 6, together with the thermodynamic parameters in Tables 4 and 6, of two steps in the oxidation process emphasize that the lower energy barrier; the easier desorption of CO<sub>2</sub> on Pt<sub>(N)</sub>-BNNT site in ER mechanism. The existence of the commonly observed linear-free-energy-type relationship, the decrease in adsorption enthalpy and other thermodynamic parameters of the two steps in the ER mechanism of CO oxidation process, are coinciding with the lower adsorption activation energy. On the other hand, E<sub>a</sub>, and C<sub>v</sub> values of the second step were always greater than those of first step at the same temperature and pressure.

In the ER-mechanism, the energy barriers at room temperature for each step in Fig. 7 are: E<sub>bar</sub> = 0.37 eV for step 1, E<sub>bar</sub> = 0.24 eV for step 2. The reaction time for each step in Fig. 7 at room temperature is calculated by the following expression,

$$\tau = \frac{1}{\nu e^{\left(\frac{-E_{\text{bar}}}{k_B T}\right)}}$$

Where  $\nu$  is in order of 10<sup>12</sup> Hz,  $k_B$  is the Boltzmann constant and  $T = 298.15$  K.  $\tau_1 = 1.98 \times 10^{-6}$  s for step 1 and  $\tau_2 = 12.83 \times 10^{-9}$  s for step 2, respectively. Consequently, the CO oxidation on Pt<sub>(N)</sub>-BNNT site following the ER reaction pathway entails lower activation barriers and higher reaction rate than that of LH pathway suggesting the superiority of the ER mechanism for CO oxidation.

Finally, it is demonstrated that the activity of nano-materials supported transition metal catalysts is strongly dependent on the dispersion and stability of TM clusters on the support [65,84–87]. To verify the possibility of clustering on BNNT substrate, the geometry and electronic structures of the defect-free and defective BN nanotube doped with the Pt cluster, e.g., Pt dimer and trimer have been investigated using DFT calculations. The binding energies (E<sub>b</sub>) of Pt<sub>n</sub> clusters on BNNT surfaces were calculated as

$$E_b = E_{\text{Pt}_{(n)}/\text{BNNT\_site}} - (E_{\text{BNNT\_site}} + E_{\text{Pt}_{(n)}})$$

where  $E_{\text{Pt}_{(n)}/\text{BNNT\_site}}$ ,  $E_{\text{BNNT\_site}}$  and  $E_{\text{Pt}_{(n)}}$  stand for the total energies of the adsorbed Pt<sub>(n)</sub> clusters (n = 2,3) at BNNT<sub>site</sub>, isolated BNNT<sub>site</sub> and Pt<sub>(n)</sub> clusters, respectively. The corresponding values of optimized structures, the binding strength of Pt clusters and charges transfer for the deposition of the Pt<sub>2</sub>, Pt<sub>3</sub> on the pristine BNNT, V<sub>B</sub> and V<sub>N</sub> sites have been summarized in Table 8.

After full geometry optimization with the various locations of second Pt atom, the most stable configurations for the adsorbed Pt dimer occupy either inclined from the surface normal (defect free and V<sub>B</sub>) or vertically (V<sub>N</sub>) relative to the surface plane. As compared with the pristine BNNT, the binding strength of Pt clusters on defective BNNT is significantly enhanced due to their strong hybridization with the vacancy site. Thus, the point defect on BNNT plays a vital role on anchoring Pt clusters, ensuring their high stability. At the pristine BNNT, the most stable configuration of Pt dimer is bound at the B-N bridge site. The Pt-Pt bond length in the adsorbed form is elongated to 2.43 Å as compared with the gas-phase bond length of 2.38 Å which coincide with the value of 2.40 Å of Pt<sub>2</sub> dimers by LDA approximation calculation [88]. The bond lengths of Pt-Pt on V<sub>B</sub> and V<sub>N</sub> defects are elongated to 2.49 and 2.56 Å, respectively. Such deformation is attributed to the strong hybridization of the Pt<sub>2</sub> cluster and the dangling bonds of the defective BNNT. The bond lengths of Pt-B and Pt-N at V<sub>B</sub> and V<sub>N</sub> defects are 2.08 and 2.11 Å, respectively which are larger than those of isolate metal-doped BNNT. This indicates that the internal interaction between the two metal atoms due to the formation of dimer weakens the metal-BNNT interaction.

Upon adsorption of Pt<sub>3</sub> cluster on BNNT substrate, the most stable configurations, structural parameters and binding energies are summarized in Table 8. For a pristine BNNT, the most stable configuration is that two Pt atoms of the Pt<sub>3</sub> cluster are attached to two B-N bridge

sites, while the third Pt atom binds directly above the adsorbed Pt atoms. The bond lengths of the Pt-N and Pt-B are greater than that of Pt<sub>2</sub> at the pristine BNNT. At the V<sub>B</sub> and V<sub>N</sub> sites, the first Pt atom is used to saturate the three dangling N or B atoms whereas the second and third Pt atoms are directly bonded to the first Pt atom. Similarly, the Pt<sub>3</sub> cluster adsorption also leads to the elongation of the Pt-Pt bond as shown in Table 8.

As shown in Table 8, the strong adsorption of Pt clusters on defective BNNT is accompanied by the large charge transfer to or from the Pt particles. Thus, the charges localized on Pt dimer that trapped by B and N vacancy are +0.64 and -0.36, respectively. The Pt trimer adsorbed on V<sub>B</sub> and V<sub>N</sub> defects possesses charge of +0.73 and -0.37, respectively. Thus, V<sub>N</sub>-BNNT donates electrons to the adsorbed Pt<sub>2</sub> and Pt<sub>3</sub>, while V<sub>B</sub>-BNNT acts as an electron acceptor. Consequently, the charge of the adsorbed Pt clusters strongly depends on the type of vacancy. Hence, it is possible to modify considerably the cluster's electron donor-acceptor capacity and its catalytic properties by the support design. The charge re-distribution of Pt nano-clusters is expected to facilitate the interaction of gases (O<sub>2</sub>, CO, OH, and H<sub>2</sub>) on Pt catalyst in fuel cells, and therefore enhance the performance of the catalytic activity in CO oxidation. This will be a topic of future research.

#### 4. Conclusions

DFT calculations have been performed to investigate the reaction mechanism of CO oxidation catalyzed by the Pt doped at BNNT (5,5) system. To gain more insight into how CO and O<sub>2</sub> interact with Pt-BNNT, the electronic structures and thermochemical properties of these two species adsorbed on Pt-BNNT with the metal embedded at the B- and N-vacancy are analyzed. The DFT calculations demonstrated that the reactivity of the defective BNNTs toward Pt atom is higher than that of the perfect BNNTs hence the intrinsic defects play a decisive role. The binding energies of a single Pt atom onto V<sub>B</sub>-BNNT and V<sub>N</sub>-BNNT are -7.21 and -6.76 eV, suggesting the diffusion of the anchored Pt atoms difficult. It is found that O<sub>2</sub> binds stronger than CO on Pt<sub>(N)</sub>-BNNT but weaker than CO on a Pt(B)-BNNT. The presence of a pre-adsorbed O<sub>2</sub> molecule on Pt<sub>(N)</sub>-BNNT surface eliminates any chance of CO poisoning of the surface. The excess of the positive or negative charge on Pt can considerably change its catalytic properties and enhance activation of the adsorbed O<sub>2</sub>. Based on the PDOS analysis, the activation is attributed to the strong hybridization between Pt-5d and the 2p orbitals of O<sub>2</sub> molecules. In addition, the results show that IR technique is a powerful tool to investigate the gas solid interface.

Finally, the CO oxidation barriers and vibrational frequency calculations in the ER mechanism with a two-step route were performed. The thermodynamics and the kinetics of CO oxidation process are remarkably similar between two steps in ER mechanism. Both reaction steps could proceed rapidly because of the low energy barriers. The results in this work suggest that Pt<sub>(N)</sub>-BNNT might be a good candidate for highly active and stable catalysts for oxidation reactions.

#### Acknowledgments

The author is grateful to Deanship of Scientific Research, Qassim University for the support of this work. My gratitude and deep thanks to Prof. Dr. A.S. Shalabi for his interest, and useful discussions.

#### References

- [1] A.A. Herzing, C.J. Kiely, A.F. Carley, P. Landon, G.J. Hutchings, *Science* 321 (2008) 1331.
- [2] X.W. Xie, Y. Li, Z.Q. Liu, M. Haruta, W.J. Shen, *Nature* 458 (2009) 746.
- [3] A. Hornes, A.B. Hungria, P. Bera, A.L. Camara, M. Fernandez-García, A. Martínez-Arias, L. Barrio, M. Estrella, G. Zhou, J.J. Fonseca, J.C. Hanson, J.A. Rodríguez, *J. Am. Chem. Soc.* 132 (2010) 34.
- [4] C.J. Huang, X.X. Ye, C. Chen, S. Lin, D.Q. Xie, *Comput. Theor. Chem.* 1011 (2013) 5.
- [5] S. Royer, D. Duprez, *Chem. Cat. Chem.* 3 (2011) 24.

- [6] M.S. Chen, Y. Cal, Z. Yan, K.K. Gath, S. Axnanda, D.W. Goodman, *Surf. Sci.* 601 (2007) 5326.
- [7] X. Liu, Y. Sui, T. Duan, C. Meng, Y. Hanb, *Catal. Sci. Technol.* 5 (2015) 1658.
- [8] W.T. Yu, M.D. Porosoff, J.G.G. Chen, *Chem. Rev.* 112 (2012) 5780.
- [9] R. Siburian, T. Kondo, J. Nakamura, *J. Phys. Chem. C* 117 (2013) 3635.
- [10] S. Shan, V. Petkov, L. Yang, J. Luo, P. Joseph, D. Mayzel, B. Prasai, L. Wang, M. Engelhard, C.-J. Zhong, *J. Am. Chem. Soc.* 136 (2014) 7140.
- [11] R. Toyoshima, M. Yoshida, Y. Monya, Y. Kousa, K. Suzuki, H. Abe, B.S. Mun, K. Mase, K. Amemiya, H. Kondoh, *J. Phys. Chem. C* 116 (2012) 18691.
- [12] M.L. Kimble, A.W. Castleman, R. Mitric, C. Burgel, V. Bonacic-Koutecky, *J. Am. Chem. Soc.* 126 (2004) 2526.
- [13] B.T. Qiao, A.Q. Wang, X.F. Yang, L.F. Allard, Z. Jiang, Y.T. Cui, J.Y. Liu, J. Li, T. Zhang, *Nat. Chem.* 3 (2011) 634.
- [14] M. Moses-DeBusk, M. Yoon, L.F. Allard, D.R. Mullins, Z. Wu, X. Yang, G. Veith, G.M. Stocks, C.K. Narula, *J. Am. Chem. Soc.* 135 (2013) 12634.
- [15] Q.G. Jiang, Z.M. Ao, S. Lib, Z. Wen, *RSC Adv.* 4 (2014) 20290.
- [16] Y.H. Lu, M. Zhou, C. Zhang, Y.P. Feng, *J. Phys. Chem. C* 113 (2009) 20156.
- [17] E.H. Song, Z. Wen, Q. Jiang, *J. Phys. Chem. C* 115 (2011) 3678.
- [18] Y.F. Li, Z. Zhou, G.T. Yu, W. Cheng, Y.F. Chen, *J. Phys. Chem. C* 114 (2010) 6250.
- [19] Y. Tang, Z. Yang, X. Dai, *Phys. Chem. Chem. Phys.* 14 (2012) 16566.
- [20] X. Liu, Y. Sui, T. Duan, C. Meng, Y. Han, *Phys. Chem. Chem. Phys.* 16 (2014) 23584.
- [21] E. Yoo, T. Okata, T. Akita, M. Kohyama, J. Nakamura, I. Honma, *Nano Lett.* 9 (2009) 2255.
- [22] Zhao, Y. Su, Y. Zhang, S.J. Li, G. Chen, *Chem. Phys. Lett.* 515 (2011) 159.
- [23] S. Lin, J. Huang, X. Ye, *Appl. Surf. Sci.* 320 (2014) 237.
- [24] K. Mao, L. Li, W. Zhang, Y. Pei, X.C. Zeng, X. Wu, J. Yang, *Sci. Rep.* 4 (2014) 5441.
- [25] X. Liu, T. Duan, Y. Sui, C. Meng, Y. Hanb, *RSC Adv.* 4 (2014) 38750.
- [26] X. Liu, T. Duan, Y. Sui, C. Meng, Y. Hanb, *RSC Adv.* 5 (2015) 10452.
- [27] M. Gao, A. Lyalin, T. Taketsugu, *J. Phys. Chem. C* 116 (2012) 9054.
- [28] N. Injan, J. Sirijaraensreb, J. Limtrakul, *Phys. Chem. Chem. Phys.* 16 (2014) 23182.
- [29] H. Orita, Y. Inada, *J. Phys. Chem. B* 109 (2005) 22469.
- [30] P. Kačer, M. Kuzma, L. Červený, *Appl. Catal. A* 259 (2004) 179.
- [31] D. Golberg, Y. Bando, C.C. Tang, C.Y. Zhi, *Adv. Mater.* 19 (2007) 2413.
- [32] C.Y. Zhi, Y. Bando, C. Tang, D. Golberg, *Mater. Sci. Eng. R. Rep.* 70 (2010) 92.
- [33] R.G. Bhimanapati, D. Kozuchab, J.A. Robinson, *Nanoscale* 6 (2014) 11671.
- [34] M. Terrones, J.M. Romo-Herrera, E. Cruz-Silva, F. López-Urías, E. Muñoz-Sandoval, J.J. Velázquez-Salazar, H. Terrones, Y. Bando, D. Golberg, *Mater. Today* 10 (2007) 30.
- [35] D. Golberg, Y. Bando, Y. Huang, T. Terao, M. Mitome, C. Tang, C. Zhi, *ACS Nano* 4 (2010) 2979.
- [36] Y. Miyamoto, A. Rubio, S. Berber, M. Yoon, D. Tomanek, *Phys. Rev. B* 59 (2004) 121413.
- [37] A. Zobelli, C.P. Ewels, A. Gloter, G. Seifer, O. Stephan, S. Csilag, C. Colliex, *Nano Lett.* 6 (2006) 1955.
- [38] H. Roohi, S. Bagheri, *Struct. Chem.* 24 (2013) 409.
- [39] S. Azevedo, J.R. Kaschny, C.M.C. Castilho, F.B. Mota, *Nanotechnology* 18 (2007) 495707.
- [40] I. Jiménez, A. Jankowski, L.J. Terminello, J.A. Carlisle, D.G.J. Sutherland, G.L. Doll, J.V. Mantese, W.M. Tong, D.K. Shuh, F.J. Himpsel, *Appl. Phys. Lett.* 68 (1996) 2816.
- [41] I. Jiménez, A.F. Jankowski, L.J. Terminello, D.G.J. Sutherland, J.A. Carlisle, G.L. Doll, W.M. Tong, D.K. Shuh, F.J. Himpsel, *Phys. Rev. B* 55 (1997) 12025.
- [42] W. Orellana, H. Chacham, *Phys. Rev. B* 63 (2001) 125205.
- [43] C. Jin, F. Lin, K. Suenaga, S. Iijima, *Phys. Rev. Lett.* 102 (2009) 195505.
- [44] L. Liu, Y.P. Feng, Z.X. Shen, *Phys. Rev. B: Condens. Matter Mater. Phys.* 68 (2003) 104102.
- [45] L. Museur, E. Feldbach, A. Kanaev, *Phys. Rev. B: Condens. Matter Mater. Phys.* 78 (2008) 155204.
- [46] R.-F. Liu, C. Cheng, *Phys. Rev. B: Condens. Matter Mater. Phys.* 76 (2007) 014405.
- [47] S.A. Shevlin, Z.X. Guo, *Phys. Rev. B: Condens. Matter Mater. Phys.* 76 (2007) 024104.
- [48] M. Petracic, R. Peter, I. Kavre, L.H. Li, Y. Chen, L.J. Fan, Y.W. Yang, *Phys. Chem. Chem. Phys.* 12 (2010) 15349.
- [49] Y. Xie, Y.P. Huo, J.M. Zhang, *Appl. Surf. Sci.* 258 (2012) 6391.
- [50] X. Wu, J.L. Yang, X.C. Zeng, *J. Chem. Phys.* 125 (2006) 044704.
- [51] R. Wang, D. Zhang, C. Liu, *Comput. Mater. Sci.* 82 (2014) 361.
- [52] M.L. Liao, Y.C. Wang, S.P. Ju, T.W. Lien, L.F. Huang, *J. Appl. Phys.* 110 (2011) 054310.
- [53] C.Y. Zhi, Y. Bando, C.C. Tang, Q. Huang, D. Golberg, *J. Mater. Chem.* 18 (2008) 3900.
- [54] X. Wu, J. Yang, J.G. Hou, Q. Zhu, *J. Chem. Phys.* 124 (2006) 054706.
- [55] W. An, X. Wu, J.L. Yang, X.C. Zeng, *J. Phys. Chem. C* 111 (2007) 14105.
- [56] R.J. Baierle, P. Piquini, T.M. Schmidt, A. Fazzio, *J. Phys. Chem. B* 110 (2006) 21184.
- [57] A.A. Peyghan, A. Soltani, A.A. Pahlevani, Y. Kanani, S. Khajeh, *Appl. Surf. Sci.* 270 (2013) 25.
- [58] X. Wu, X.C. Zeng, *J. Chem. Phys.* 125 (2006) 044711.
- [59] Y.K. Chen, L.V. Liu, Y.A. Wang, *J. Phys. Chem. C* 114 (2010) 12382.
- [60] S. Lin, X. Ye, J. Huang, *Phys. Chem. Chem. Phys.* 17 (2015) 888.
- [61] A.D. Becke, *Phys. Rev.* 38 (1988) 3098.
- [62] C. Lee, W. Yang, R.G. Parr, *Phys. Rev. B* 37 (1988) 785.
- [63] M.J. Frisch, et al., *Gaussian 09*, Gaussian Inc., Pittsburgh, PA, 2009.
- [64] N.M. O'Boyle, A.L. Tenderholt, K.M. Langner, *J. Comput. Chem.* 29 (2008) 839.
- [65] D. Xu, Y.J. Liu, J.X. Zhao, Q.H. Cai, X.Z. Wang, *J. Phys. Chem. C* 118 (2014) 8868.
- [66] S. Lin, X. Ye, R.S. Johnson, H. Guo, *J. Phys. Chem. C* 117 (2013) 17319.
- [67] A.J. Du, Y. Chen, Z.H. Zhu, R. Amal, G.Q. Lu, S.C. Smith, *J. Am. Chem. Soc.* 131 (2009) 17354.
- [68] G.Y. Gou, B.C. Pan, L. Shi, *Phys. Rev. B* 76 (2007) 155414.
- [69] X. Blase, A. Rubio, S.G. Louie, M.L. Cohen, *Europhys. Lett.* 28 (1994) 335.
- [70] X. Blase, L.X. Benedict, E.L. Shirley, S.G. Louie, *Phys. Rev. Lett.* 72 (1994) 1878.
- [71] X. Blase, A. DeVita, J.C. Charlier, R. Car, *Phys. Rev. Lett.* 80 (1998) 1666.
- [72] J.X. Zhao, Y.H. Ding, *J. Chem. Phys.* 131 (2009) 014706.
- [73] H. Heyne, F.C. Tompkins, *Trans. Faraday Soc.* 63 (1967) 1274.
- [74] X. Feng, M. Yao, X. Hub, G. Hu, A. Jia, G. Xie, J. Lu, M. Luo, *Int. J. Hydrog. Energy* 38 (2013) 13673.
- [75] C.S. Yeung, L.V. Liu, Y.A. Wang, *J. Theor. Comput. Nanosci.* 4 (2007) 1108.
- [76] J.L.C. Fajín, M.N.D.S. Cordeiro, J.R.B. Gomes, *Appl. Catal. A* 379 (2010) 111.
- [77] A. Lyalin, T. Taketsugu, *J. Phys. Chem. C* 113 (2009) 12930.
- [78] A. Lyalin, T. Taketsugu, *J. Phys. Chem. Lett.* 1 (2010) 1752.
- [79] J. Hagen, L.D. Socaciu, J. Le Roux, D. Popolan, T.M. Bernhardt, L. Wöste, R. Mitrić, H. Noack, V. Bončić-Koutecký, *J. Am. Chem. Soc.* 126 (2004) 3442.
- [80] M. Gao, A. Lyalin, T. Taketsugu, *J. Chem. Phys.* 138 (2013) 034701.
- [81] <http://www.spectralcalc.com>.
- [82] K.J. Laidler, *Pure Appl. Chem.* 68 (1996) 149.
- [83] W. An, Y. Pei, X.C. Zeng, *Nano Lett.* 8 (2008) 195.
- [84] Q. Sun, Q. Wang, P. Jena, Y. Kawazoe, *J. Am. Chem. Soc.* 127 (2005) 14582.
- [85] S. Li, P. Jena, *Phys. Rev. Lett.* 97 (2006) 209601.
- [86] R. Kou, Y.Y. Shao, D.H. Mei, Z.M. Nie, D.H. Wang, C.M. Wang, V.V. Viswanathan, S. Park, I.A. Aksay, Y.H. Lin, Y. Wang, *J. Am. Chem. Soc.* 133 (2011) 2541.
- [87] W. Gao, J.E. Mueller, J. Anton, Q. Jiang, T. Jacob, *Angew. Chem. Int. Ed.* 52 (2013) 14237.
- [88] E.Y. Zarechnaya, N.V. Skorodumova, S.I. Simak, B. Johansson, E.I. Isaev, *Comput. Mater. Sci.* 43 (2008) 522.